

Solvent-Induced Degradation of Electrochemically Exfoliated Vanadium Selenide Visualized by Electron Microscopy

Sarah Friedensen,[†] Parisa Yasini,[†] Rachael Keneipp, Alice Castan, and Marija Drndić*Cite This: *ACS Omega* 2022, 7, 42146–42154

Read Online

ACCESS |



Metrics & More

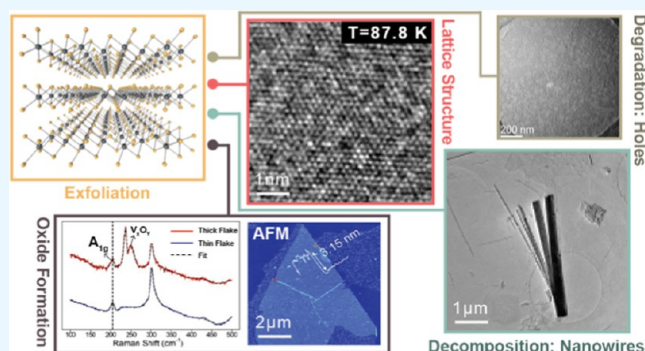


Article Recommendations



Supporting Information

ABSTRACT: Recently discovered two-dimensional ferromagnetic materials (2DFMs) have rapidly gained much interest in the fields of spintronics and computing, where they may prove powerful tools for miniaturizing devices such as magnetic tunnel junctions and spin-transfer torque memory bits. In addition, heterojunctions and twisted bilayer stacks of such materials may yield exotic spin textures. However, preparation of such devices is complicated by the air sensitivity of many 2DFMs. Here, we report details on the preparation of few-to-monolayer flakes of vanadium selenide (VSe_2) using electrochemical exfoliation in propylene carbonate. We also present a detailed study of the effects of air on the structure and magnetic properties of bare and passivated VSe_2 after different concentrations of surface passivation treatment. We characterized the microstructure of holes in the VSe_2 flakes and the formation of new compounds arising from air exposure, solvent exposure during the exfoliating process, and deliberate electron beam irradiation (sculpting). We sculpt VSe_2 flakes while retaining the 1T- VSe_2 lattice structure, opening the door for top-down patterned high-resolution 2DFM nanostructures. Additionally, investigation of the magnetic response of nanosheets using magnetic force microscopy (MFM) showed that the oxidation-induced damage only affects the surface fields locally and does not quench large-scale magnetic signal. The findings of this study pave the way toward practical incorporation of 2D ferromagnetic materials in nanoelectronics.



1. INTRODUCTION

Two-dimensional (2D) transition-metal dichalcogenides (TMDs) VX_2 ($X = \text{S}, \text{Se}$) and their heterostructures have been suggested to exhibit rich and unique electronic properties including confinement-induced charge-ordered states, superconductivity, ferromagnetism, and Curie temperatures (T_C) considerably above room temperature,^{1–6} making them extremely promising for room-temperature quantum and spintronic applications. Developing these applications requires the structural characterization of 2D materials and investigation of two main aspects of these materials: their properties under dimensional reduction from bulk to 2D, 2D to one-dimensional (1D), and the emergent phenomena induced by stacking these materials in multilayers. While in recent years the field of quantum devices has progressed from exploratory work to implementation, the cryogenic temperatures required for operation may limit practical applications. Through clever preparation techniques, the realization of novel spin textures and dynamics in materials such as VX_2 may be possible, which motivates investigations into new preparation techniques and methods of enhancing environmental stability.

Bulk vanadium selenide (VSe_2) has primarily been known for its unique three-dimensional (3D) charge density wave (CDW) transition at approximately 110 K due to 3D Fermi surface “nesting,” with the exact transition temperature

depending on material thickness.^{7–13} Recently, however, investigation of its electronic and magnetic properties has begun to gain attention, which has led to both controversy and practical challenges. Some theoretical studies have shown that VSe_2 exhibits ferromagnetic behavior in the few- to monolayer limit, with a predicted Curie temperature of 472 K.³ In addition, recent experimental studies have shown the emergence of ferromagnetic ordering stable above room temperature.² However, the existence of intrinsic ferromagnetism in VSe_2 has been called into question by recent experimental studies that report no ferromagnetic signal from VSe_2 monolayer film at temperatures down to 10 K using X-ray magnetic circular dichroism (XMCD) experiments.^{14,15} Using the same technique, another study showed the absence of a long-range magnetic order at temperatures down to 2 K and magnetic fields up to a 7 T in VSe_2 monolayers.¹⁶

Received: July 27, 2022

Accepted: October 26, 2022

Published: November 9, 2022



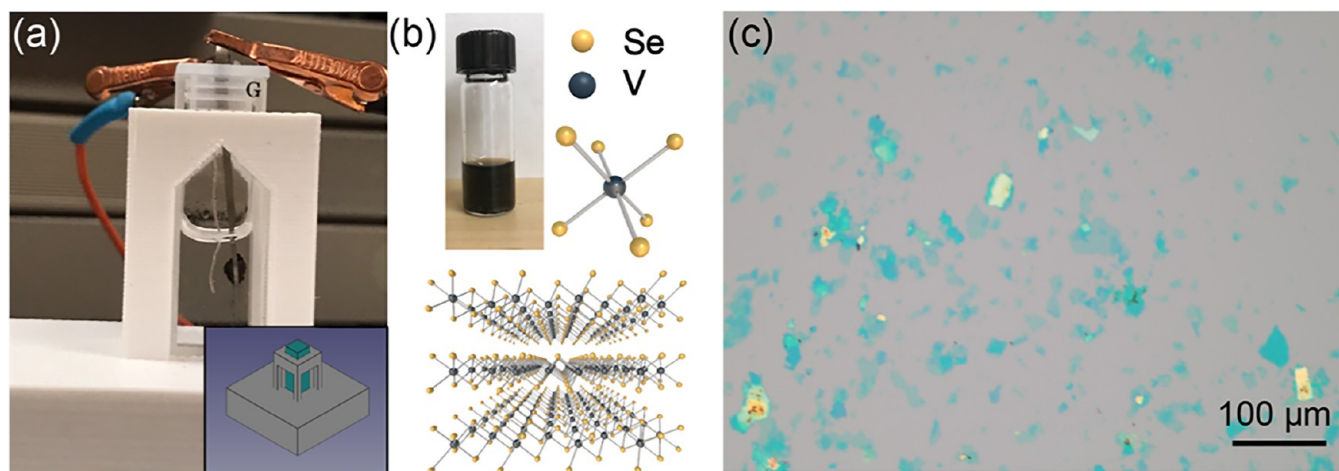


Figure 1. Exfoliation of ultrathin VSe_2 : (a) Exfoliation setup, including 3D-printed cuvette holder (CAD inset), glass cuvette containing propylene carbonate, tetrapropylammonium chloride, platinum electrode, and titanium hook electrode holding bulk VSe_2 flake. (b) Propylene carbonate containing exfoliated VSe_2 flakes and atomic structure of exfoliated 1T- VSe_2 layers. (c) Optical image of exfoliated VSe_2 flakes drop-cast onto Si/ SiO_2 wafer fragment.

In addition to the above-mentioned debate, obtaining robust, large-area monolayer flakes of VSe_2 present some difficulties. Mechanical exfoliation down to monolayers is challenging possibly due to relatively strong attractive forces between the monolayer and the polymer or the tape used for peeling.¹⁷ In addition, ultrathin VSe_2 flakes are extremely unstable in air, due to the oxidation of Se vacancies.¹⁸ Several avenues have been explored in efforts to attain monolayer VSe_2 , including molecular beam epitaxial (MBE) growth,^{2,19} mechanical exfoliation from bulk crystals,^{9,20,21} chemical vapor deposition (CVD) growth,^{8,10,21–24} colloidal synthesis,^{25–28} liquid-phase exfoliation,⁷ and electrochemical exfoliation.¹⁸ In addition, after successful isolation of ultrathin layers of materials, aging and degradation are important aspects that need to be considered for further practical applications and device performance. For example, aging of 2D transition-metal dichalcogenides over several months showed changes in morphology and severe quenching of the direct gap photoluminescence, which could be prevented by encapsulation of the monolayer sheet by an ~ 10 nm thick polymer.^{29,30}

Recently, preparation of ultrathin VSe_2 has been reported using electrochemical exfoliation and surface passivation with $1\text{H},1\text{H}_2,2\text{H}_2,2\text{H}$ -perfluorodecanethiol (FDT, $\text{C}_{10}\text{H}_5\text{F}_{17}\text{S}$).¹⁸ This study supported the existence of a ferromagnetic response in room-temperature VSe_2 and demonstrated that passivation with FDT protected against oxidation.¹⁸ In this paper, we conduct a detailed study of ultrathin 1T-phase VSe_2 flakes obtained via this electrochemical exfoliation technique. We further investigate and expand upon the previous exfoliation protocol and study the properties of the resulting flakes. In this study, we highlight the development and effects of holes and other defects developed during the exfoliation process, the air stability of the as-prepared VSe_2 flakes, and the concentration-dependent effect of chemical passivation with dilute FDT using atomic and magnetic force microscopy (AFM and MFM). In addition, the defects induced by solvent and electron beam have been investigated using transmission electron microscopy (TEM) down to cryogenic temperatures (see Supporting Information, SI Figure S1) and electron-dispersive X-ray spectroscopy (EDS). We find that when ultrathin flakes of VSe_2 oxidize, the oxide forms small pillars on top of the flake.

Additionally, we demonstrate the suitability of VSe_2 ultrathin flakes for TEM nanosculpting and take the solvent-mediated decomposition of VSe_2 in propylene carbonate (PC) to its logical extreme and identify the decomposition products.

2. METHODS

High-purity bulk VSe_2 was purchased from 2D semiconductors and stored under vacuum until ready for use. Following the procedure established by Yu et al.,¹⁸ we prepared few-layer to monolayer samples of VSe_2 via electrochemical exfoliation. The electrolyte solution was composed of 5 mM tetrapropylammonium chloride (TPAC, Sigma-Aldrich, 98%) dissolved in propylene carbonate (PC, Sigma-Aldrich, 99.7%). The VSe_2 cathode was held by a bent strip of titanium foil (Figure 1a), and platinum wire served as the anode. The reaction took place in a glass cuvette. To drive tetrapropylammonium cation (TPA^+) intercalation and exfoliation, voltages between 2 and 2.5 V were applied, with exfoliation of the flakes selected for study occurring at 2.5 V for 30 min. The expanded VSe_2 crystal was removed to a fresh solution of PC after turning completely black and visibly expanding (Figure 1a). After manually shaking the resultant solution until it appeared well dispersed and then sonicating the black suspension for 1–2 min (Figure 1b, top), the solution was transferred to an argon glovebox and immediately drop-cast.

Piranha-cleaned silicon wafer fragments coated with 300 nm of thermal silicon oxide (Figure 1c) and fresh holey carbon grids were used as substrates for the exfoliated flakes for AFM/MFM measurements and TEM experiments, respectively. These samples were then immediately transferred to the vacuum antechamber of the glovebox attached to an Edwards RV12F rotary-vane pump to dry overnight (for the quick drying experiment—see SI Figure S2—an Edwards nXDS 6i scroll pump was used instead), except in the case of the grid used for cryogenic TEM. After drying, bare VSe_2 grids were transported to a JEOL F200 TEM under argon and quickly loaded into the TEM for atomic-resolution imaging. The cryo-TEM grid was loaded into the Gatan Ultra Low Temperature Double Tilt (ULTDT) liquid helium TEM holder immediately after drop-casting with the propylene carbonate VSe_2 suspension and while still wet, then placed under high vacuum

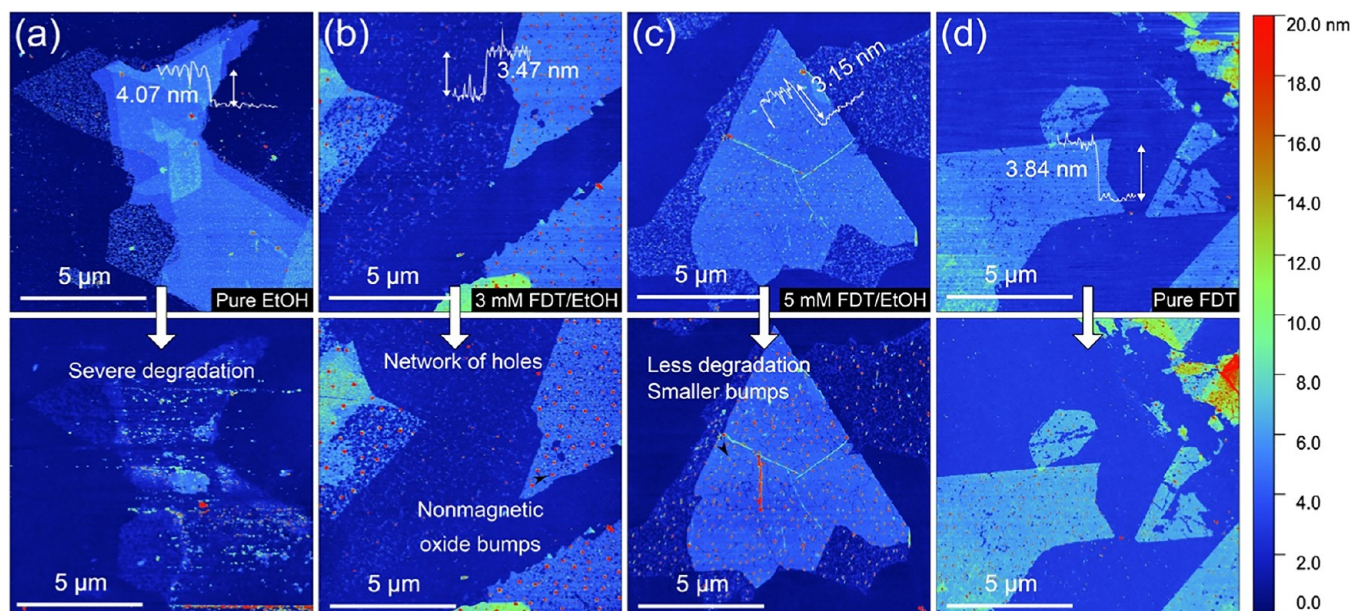


Figure 2. Atomic force microscope topography of VSe₂ flakes treated with (a) pure ethanol, (b) 3 mM C₁₀H₅F₁₄S in ethanol, (c) 5 mM C₁₀H₅F₁₄S in ethanol, and (d) pure C₁₀H₅F₁₄S at roughly 0 (top) and 24 (bottom) hours.

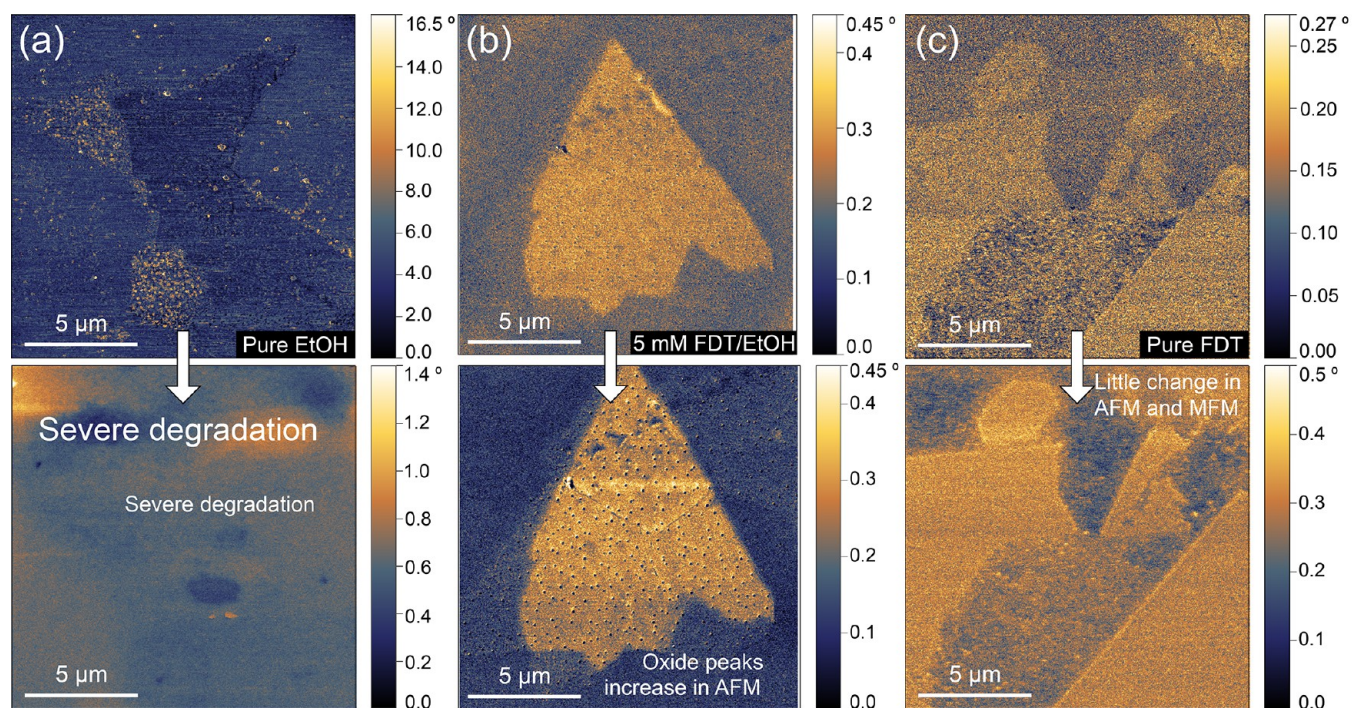


Figure 3. Magnetic force microscopy phase of VSe₂ flakes treated with (a) pure ethanol, (b) 5 mM C₁₀H₅F₁₄S in ethanol, and (c) pure C₁₀H₅F₁₄S at roughly 0 (top) and 24 (bottom) hours. In (a), the features in the top quarter of the 24 h image are not associated with any topography and are suspected to be spurious instrument fluctuations. In (c), note that after passing over a high feature in the approximate center of the first scan, the contrast inverted at the horizontal line. The authors have inverted the contrast again for easier viewing, but noncorrected data are available as the [Supporting Information](#). The contrast change between 0 and 24 h is due to the AFM realignment.

overnight. For surface passivation, FDT (97% Sigma-Aldrich) was used on its own as well as diluted to the following concentrations in ethanol: undiluted, 5 mM, and 3 mM. Control samples were treated with pure ethanol. All samples were immersed in their treatment solutions overnight and then washed with acetone. AFM/MFM samples were then quickly dried in air with a nitrogen gun before being returned to the argon glovebox, whereas TEM grids were allowed to dry

evaporatively under argon. Immediately prior to AFM and MFM measurement, samples were immersed and gently agitated in isopropanol for 10 min before blow-drying and mounting on magnetic sample pucks. Before TEM measurements, grids were rinsed in methanol and dried under argon.

Atomic and magnetic force microscopy measurements were performed with a Bruker MultiMode8 AFM in air to determine the extent of VSe₂ degradation in atmosphere over a span of 24

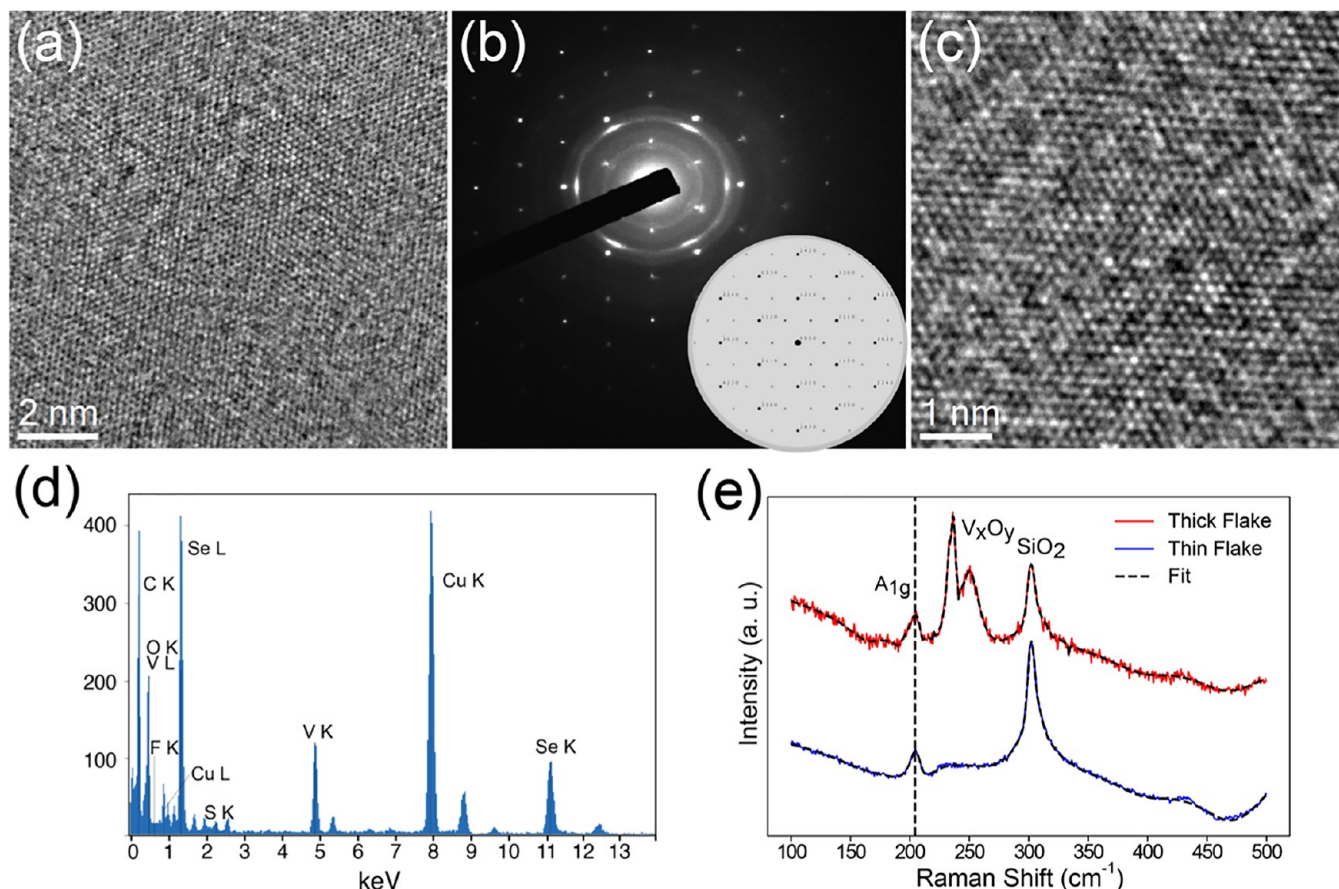


Figure 4. TEM and Raman analysis of bare VSe_2 . (a) Room-temperature HR-TEM of suspended thin VSe_2 , showing lattice spacing of 0.311 nm. (b) Room-temperature diffraction of suspended thick VSe_2 with simulation inset. The diffusion in FFT could be due to solvent contamination and oxide formation. (c) 87.8 K HR-TEM image of suspended thin VSe_2 with lattice spacing of 0.305 nm. (d) EDS spectrum of bare VSe_2 on holey carbon copper grid, showing vanadium and selenium as well as a miniscule sulfur peak, but no fluorine. (e) Raman spectra of thick (red) and thin (blue) bare VSe_2 flakes on Si/SiO_2 wafer fragment.

h. At the time of measurement, the exfoliated samples shown had been stored in the glovebox for four months. However, topography measurements on samples prepared from a new exfoliation and measured within the same week behaved similarly (SI Figure S2). Topography measurements were taken using Bruker's PeakForce HR mode and associated tips. For MFM, Bruker MESP-V2 tips were used. The MESP-V2 tips were magnetized with a lateral field in a custom holder (SI Figure S2 and supplementary .stl files) for 10 min before being loaded. For the first MFM scan, the magnetized tip was set to the highest lift height at which good contrast was achieved, and the scan taken the next day maintained that lift height, typically around 20 nm.

TEM data were taken at 200 kV in a JEOL F200 high-resolution transmission electron microscope (HR-TEM) in phase contrast, selected-area electron diffraction (SAED), and scanning transmission electron microscopy (STEM) modes. EDS mapping and analysis were performed in Digital Micrograph.

Raman spectroscopy of the bare and 5 mM FDT-passivated VSe_2 nanoflakes on Si/SiO_2 substrates was performed under 785 nm laser excitation. Spectroscopy was performed on the same bare and 5 mM FDT-passivated flakes that were used for the AFM and MFM time series, and spectra were collected after the AFM and MFM measurements had taken place.

3. RESULTS AND DISCUSSION

3.1. Atomic and Magnetic Force Microscopy (AFM and MFM). Figure 2 shows the results of topography scans for samples treated with (a) pure ethanol, (b) 3 mM FDT in ethanol, (c) 5 mM FDT in ethanol, and (d) pure FDT. Severe degradation of the control flake is apparent: only the very thickest parts of the flake remain intact, while the rest of the area has become a loose debris field. During the first day of measurements on the control flake, substantial debris built up along the edges of the scanned region, which can be seen in the lower half of Figure 2a. The 3 mM FDT-treated sample shown in Figure 2b also degraded significantly, with the "lacy" areas becoming lacier and a larger network of holes opening in the thin flakes on the right side of the image. Additionally, the small bumps that can be seen on the flakes (red) grew larger. The 5 mM FDT-treated flakes showed less degradation in the lacy areas with holes and smaller presumptive vanadium oxide towers (Figure 2c). In addition, the few-layer flakes did not decompose into a network of holes as the 3 mM-treated flakes had. Finally, the sample treated with pure FDT (Figure 2d) shows very little change over the span of 24 h, with only the appearance of small bumps similar to those seen on the 3 mM-treated flakes being observed as a noticeable difference. These regions were observed even after extremely brief periods in air and regardless of passivation technique. This agrees with the findings of Yu et al. that show the damage accrued with time

spent in the PC suspension increases.¹⁸ SI Figure S2 supports this conclusion, as the sample shown dried faster than the other samples. This decreased both the drying time and the observed damage to the very thinnest flakes. Indeed, a monolayer region with relatively few holes can be seen in the bottom left part of SI Figure S2a,b.

Figure 3 shows the same time series with MFM scans of the ethanol control, 5 mM FDT-passivated, and pure FDT-passivated samples. Initially, the control flake shows strong signal in the lacy monolayer areas and at high peaks in the scanned region. The main body of the flake and some of its surface features are readily distinguishable from background but are dwarfed by the monolayer lacy and high-peak areas. The main body of the flake is about was measured to be 4 nm thick. At the same settings, the MFM signal of the control flake decreased by about one order of magnitude after 24 h and, other than the large central patch that also remains in the topography, is nearly indistinguishable from background. The 5 mM FDT-treated sample in Figure 3b shows that the observed topographical peaks, hypothesized to be oxidation, increase overnight in air but only locally suppress the magnetic response without affecting the rest of the flake. In addition, the surface fields from the lacelike degraded areas can be seen, strengthening our conclusion that while complete oxidation almost destroys the magnetic signal, more moderately damaged VSe₂ retains some virtue, consistent with the transport results presented by Yu et al.¹⁸ Finally, in Figure 3c, we can see that there has also been little to no discernible degradation of the magnetic signal, as expected since little to no damage was discernible in the topography.

3.2. Materials Analysis of Bare VSe₂. To verify the structure of the exfoliated material, some of the VSe₂ suspension was immediately drop-cast onto holey carbon grids for atomic-resolution TEM imaging. As can be seen in Figure 4a,b, the crystal structure of the flake is hexagonal, and measurement of the high-resolution images viewed down the [001] zone axis yields a lattice constant of 0.311 (±0.004) nm, which compares favorably with a literature value of 0.336 nm measured using XRD.⁷ Figure 4c shows an HR-TEM image of bare VSe₂ at 87.8 K, which has a smaller lattice spacing of 0.305 (±0.001) nm. These ranges are reported based on the lattice constants measured using fast Fourier transform (FFT) of the entire TEM images and the numbers are extracted using a script written in python “HexDiff” based on Miller indices indexing. This code is available upon request (see SI Figure S4 for FFTs of the entire images). The ultralow temperature TEM imaging was performed to study charge density waves (CDW). However, we did not observe any superlattice associated with the CDWs, possibly due to the thickness-dependent and solvent residue on the flakes. The small difference between the obtained lattice constant of VSe₂ at room temperature and 87.8 K could be due to a distortion in lattice structure at lower temperatures, possibly in response to the CDW transition around 110 K.^{9,31} However, further study should be conducted to confirm that this change in the in-plane lattice constant is due to the CDW. The EDS spectrum shown in Figure 4d, meanwhile, shows the presence of vanadium, selenium, and oxygen,⁴ as well as background carbon, copper, and zinc. Figure 4e compares the Raman spectra for thick and thin untreated VSe₂ flakes (see SI Figure S5 for optical images). The characteristic vibration peak appearing at 206 cm⁻¹ corresponds to the A_{1g} mode of 1T-VSe₂.^{18,20,23} The peaks at 236 and 249 cm⁻¹, meanwhile, indicate the presence of

vanadium oxides,^{23,24} supporting the hypothesis that the “towers” appearing in the AFM topography correspond to oxide formation. It is worth mentioning that according to the previous study by Yu et al. and the topography images in this study the oxide towers are present in all samples that were exposed to air whether treated or untreated. However, the oxides were more pronounced and observable using the Raman microscope on the thicker flakes, enabling us to resolve the oxide peak in the Raman spectra of the thicker samples.

Figure 5 shows HR-TEM images of VSe₂ flakes from the same grid as shown in Figure 4 after approximately 12 h air

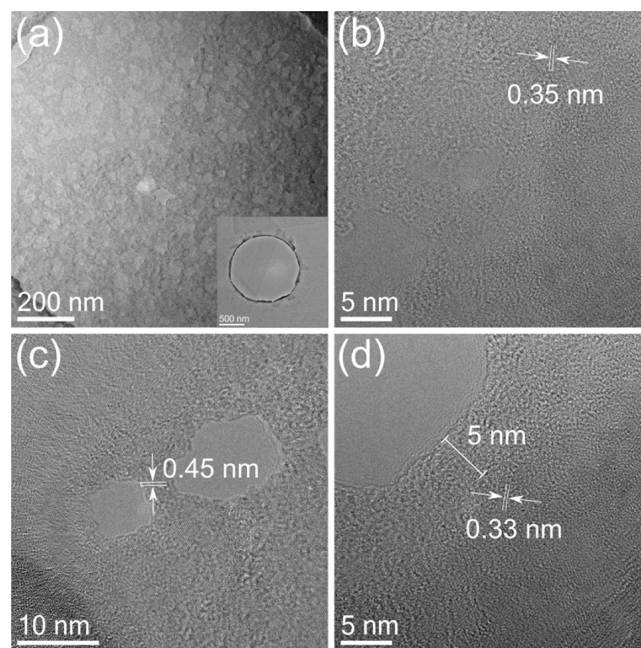


Figure 5. Oxidation damage and both naturally occurred and deliberately sculpted structures using electron beam irradiation appeared in bare VSe₂ with approximately 12 h air exposure. (a) Low-magnification image of air-exposed VSe₂ flake over carbon grid, showing many patches where material has oxidized. A bare, unoxidized flake is shown in the inset for comparison. (b) HR-TEM image of oxidized region adjacent to crystalline VSe₂. Crystalline region has a lattice spacing of 0.35 nm. (c) “Nanobridge” found in the damaged region of air-exposed VSe₂, showing a lattice spacing of 0.45 nm, potentially indicating the presence of orthorhombic vanadium oxides.³² (d) Edge of a pore drilled by rapidly bringing the beam to crossover in high-resolution TEM mode. There is an approximately 5 nm region of amorphous material between the pore itself and crystalline hexagonal VSe₂ with a lattice spacing of 0.33 nm. Lattice spacing was measured directly using a line profile on the region of interest (close to the beam-affected area).

exposure. The patchiness of the suspended flake in Figure 5a contrasts dramatically with the inset image, which shows a freshly prepared VSe₂ flake that was placed in the TEM directly without time to oxidize. The semioxidized region shown in Figure 5b appears amorphous and appears primarily around complete holes in the material. Such holes in the VSe₂ flakes arise from both air exposure and electron beam irradiation. In Figure 5c, a “nanobridge” was located that may, with a lattice constant of 0.45 nm, be composed of orthorhombic V₂O₅.³² It also proved possible to drill through the VSe₂ flake and create a pore in high-resolution mode—the beam was brought to crossover and idled for approximately one to three second

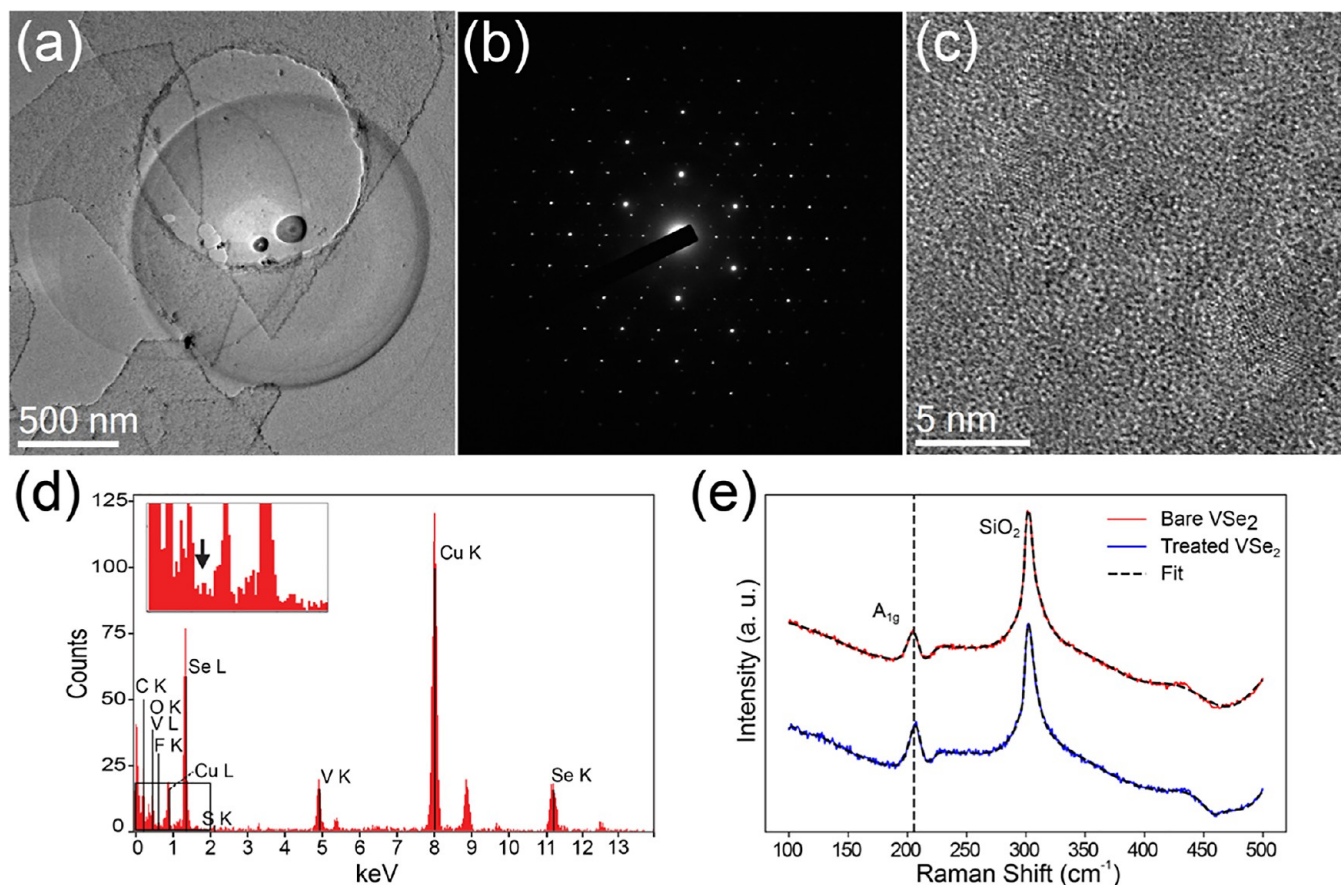


Figure 6. Analysis of passivated VSe₂. (a) Phase contrast TEM of suspended VSe₂ treated with pure C₁₀H₅F₁₄S, showing extensive carbon contamination from higher-magnification imaging (dark circles), STEM spot mode (black ovals), and beam damage. (b) Diffraction pattern of 5 mM-treated thin VSe₂ flake. (c) HR-TEM image of suspended VSe₂ flake treated with pure C₁₀H₅F₁₄S. Amorphous regions due to carbon contamination of the surface are abundant, but it is possible to obtain a lattice spacing of 0.324 nm from noncovered areas of the sample. (d) EDS of 5 mM C₁₀H₅F₁₄S-treated sample post RTA, showing vanadium and selenium, as well as small fluorine and sulfur peaks; inset: zoomed-in spectra pointing out to the fluorine K line. (e) Comparison of bare (red) and 5 mM C₁₀H₅F₁₄S-treated (blue) VSe₂ Raman spectra.

before re-spreading (beam current $\sim 150\text{--}200$ pA/cm²). Figure 5d shows the result of this experiment: the pore was surrounded by an approximately 5 nm region of amorphous material, but beyond that band, the material evidently remained 1T-VSe₂ with a lattice constant of 0.331 nm. Controlled hole formation in a ferromagnetic 2D material may present interesting opportunities for *in situ* sensing of local electromagnetic fields and engineering of new spin textures.

3.3. Materials Analysis of FDT-Treated VSe₂. Similar material analysis was also performed on VSe₂ flakes treated with FDT, as shown in Figure 6. The most defining feature of the FDT-treated samples during TEM analysis was extensive carbon contamination: the dark rings and fully black ovals that can be seen in Figure 6a are due to carbon contamination on a grid treated with pure FDT and then washed with acetone and isopropanol from viewing the imaged region under higher magnification and STEM mode, respectively. Figure 6b shows a diffraction pattern from a sample treated with 5 mM FDT, rinsed in acetone and isopropanol, and then run through a rapid thermal annealing (RTA) cycle at 350 °C to remove excess carbon so that EDS analysis could be performed without carbon contamination building up to the point that it heavily obscured the imaging region.

Despite the significant challenge, we were able to collect an HR-TEM image of the pure-FDT-treated sample that had not

undergone RTA, as shown in Figure 6c, and obtained a lattice constant of 0.324 (± 0.002) nm. Figure 6d shows the EDS spectrum results for the 5 mM FDT-treated and annealed flake (EDS for an unannealed flake can be found in SI Figure S7): In addition to the previously detected elements, a notable fluorine K line appears, indicating the presence of the FDT fluorocarbon. The sulfur signal remains quite small—this is unsurprising due to the stoichiometry of the FDT molecule. Figure 6d compares the Raman spectra of bare VSe₂ flakes and 5 mM FDT-treated VSe₂ flakes. No shift in the A_{1g} peak of VSe₂ was observed, but the peak appeared somewhat larger for the treated flakes. This difference may be attributed to differences in flake thickness.

3.4. Materials Analysis of Aged Suspension. To further investigate the effects of extended exposure to PC on VSe₂, we prepared a holey carbon TEM grid with exfoliated VSe₂ that had spent 48 h in PC suspension after chemical exfoliation (aged suspension). Fewer VSe₂ flakes were observed than in younger suspensions, and those that were found appeared thicker in the electron microscope, were often damaged, and had high sensitivity to further beam damage. Specifically, we observe that upon electron irradiation, the aged flakes were damaged more easily and over a shorter time period than the freshly deposited flakes (Figure 7). The possible reason for this observation could be the presence of holes and defects in the

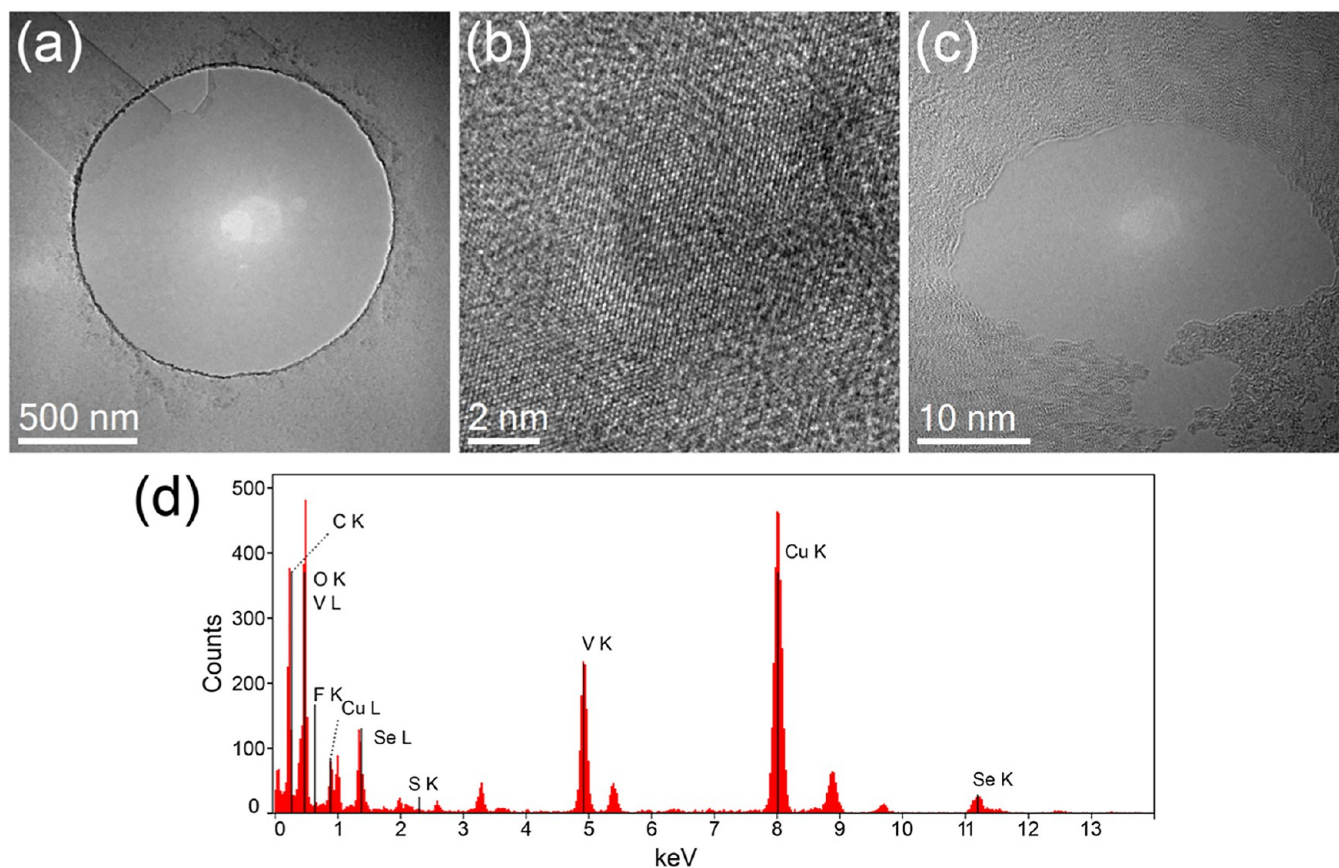


Figure 7. TEM analysis of VSe_2 flake from 48 h old propylene carbonate suspension. (a) Low-magnification image of analyzed VSe_2 flake. (b) HR-TEM image of the flake, showing a lattice spacing of 0.319 nm. (c) Example of inherent and beam-induced damage to the VSe_2 flake. Central defect began small and expanded rapidly during imaging. (d) EDS analysis of VSe_2 flake.

materials induced by solvent that are more prone to damage and expansion by electron beam compared to pristine and hole-free flakes. The accrued damage is likely to make the flake structurally weak, and a large network of preexisting defects means that fewer bonds need to be broken for the expansion of defects/holes the authors witnessed to occur (Figure 7). TEM and EDS analyses of these flakes are presented in Figure 7. The HR-TEM images obtained from these flakes nonetheless demonstrated a lattice spacing of 0.319 (± 0.004) nm (Figure 7), which remains consistent with the published value for VSe_2 .⁷ It is worth mentioning that these damaged flakes were not the only solids to appear in the aged solution. Both rectangularly symmetric nanowires and highly porous “chunks” with a network of circular holes were found on the same grid. SI Figure S8 shows TEM and EDS analysis of a few of the nanowires. It can be seen in SI Figure S8a that the nanowires are numerous, rectangular in shape, and can be several microns in size. The HR-TEM image in SI Figure S8b and its associated FFT in SI Figure S8c confirm the rectangular symmetry, and a lattice spacing of 0.45 nm is observed. This measurement agrees with published values for selenium nanowires.³³ Our hypothesis that the rectangular crystals are primarily elemental selenium gains support from the EDS maps shown in SI Figure S8d–f. The vanadium in the region of the nanowire is suppressed, while the selenium signal is atypically strong, as one would expect for a selenium crystal precipitated atop a damaged VSe_2 flake.

While we were unable to determine lattice constants from the highly porous chunks (SI Figures S8g and S9) due to the

combination of both polycrystalline and amorphous materials, EDS maps of the porous chunks in SI Figure S8g, shown in SI Figure S8h,i, are more telling. The vanadium signal from the selected region is extremely strong, and the selenium signal is quite weak, which is the reverse of what one would expect from VSe_2 based on its stoichiometry. Based on these observations, it is likely that when kept in propylene carbonate for relatively little time, VSe_2 nanoflakes decompose into their elemental constituents. This observation further supports the solvent (PC) effect and provides additional information on the degradation products.

4. CONCLUSIONS

In this work, we have confirmed the ability to electrochemically exfoliate ultrathin VSe_2 flakes including monolayers. We characterized the oxidation and degradation of the resultant flakes using atomic-resolution TEM down to cryogenic temperatures, AFM, and Raman spectroscopy. Additionally, we used MFM to explore changes in the observed magnetic response due to the formation of hole defects and putative oxide towers over time. Our results show that both propylene carbonate (PC) and oxidation damage only locally affect the surface fields measured by MFM rather than leading to wide-scale quenching of the MFM signal. We also demonstrated the ability to use an electron beam to sculpt VSe_2 nanosheets, which opens the way toward controllable TEM defect engineering and nanopatterning.

We have also expanded upon process parameters that affect the quality of electrochemically exfoliated VSe_2 ultrathin flakes:

any delay in removing the solvent, including drying time, contributes to the degradation of monolayer and bilayer regions of the flakes. This degradation initially manifests as a lacelike network of holes and eventually progresses to wide-scale decomposition of the VSe₂ into selenium nanowires and a porous sponge consisting primarily of vanadium. Damage can be mitigated by performing the exfoliation and drop-casting process quickly and minimizing the drying time. Regardless, changing to an electrolyte solvent with a higher vapor pressure and lower reactivity may be a more fruitful avenue for reliably producing quality ultrathin VSe₂ flakes.

Additionally, we determined that dilute FDT passivation can be performed with concentration-dependent efficacy and that the previously reported method of a simple acetone rinse is insufficient for removing excess FDT.¹⁸ In addition, a rapid thermal annealing cycle proved necessary to collect meaningful TEM data without massive carbon contamination. Device applications will likely require similar processing for clean electrical contact. This study provides a detailed, multipronged structural analysis of 2D VSe₂ during preparation and deposition on substrates and during top-down TEM nanofabrication, providing necessary insights for correlating structure with material properties and further advancing studies and applications of a novel 2D ferromagnetic material.

■ ASSOCIATED CONTENT

SI Supporting Information

The Supporting Information is available free of charge at <https://pubs.acs.org/doi/10.1021/acsomega.2c04749>.

Additional cryogenic phase contrast transmission electron microscope (TEM) images of VSe₂ (Figure S1); topography of VSe₂ electrochemically exfoliated and dried using an Edwards nXDS 6i scroll pump, treated with 5 mM C10H5F14S, and measured the same week as preparation (Figure S2); apparatus used for magnetizing atomic force microscope (AFM) tips and samples (Figure S3); HR-TEM images of bare VSe₂ measured (Figure S4); optical images of thinner and thicker VSe₂ flakes characterized by Raman spectroscopy (Figure S5); zoomed-in EDS spectrum of the bare VSe₂ on holey carbon copper grid, demonstrating overlap between vanadium L line and oxygen K line (Figure S6); EDS mapping of unannealed VSe₂ flake treated with 5 mM C10H5F14S in ethanol (Figure S7); and TEM analysis of nanowires and porous chunks that form in 2-day-old VSe₂ suspension in PC (Figure S8) (PDF)

Crystallographic data (ZIP)

■ AUTHOR INFORMATION

Corresponding Author

Marija Drndić – Department of Physics and Astronomy, University of Pennsylvania, Philadelphia, Pennsylvania 19104, United States; orcid.org/0000-0002-8104-2231; Email: drndic@physics.upenn.edu

Authors

Sarah Friedensen – Department of Physics and Astronomy, University of Pennsylvania, Philadelphia, Pennsylvania 19104, United States; orcid.org/0000-0002-8729-6072

Parisa Yasini – Department of Physics and Astronomy, University of Pennsylvania, Philadelphia, Pennsylvania 19104, United States; orcid.org/0000-0001-8072-6597

Rachael Keneipp – Department of Physics and Astronomy, University of Pennsylvania, Philadelphia, Pennsylvania 19104, United States

Alice Castan – Department of Physics and Astronomy, University of Pennsylvania, Philadelphia, Pennsylvania 19104, United States

Complete contact information is available at:

<https://pubs.acs.org/10.1021/acsomega.2c04749>

Author Contributions

[†]S.F. and P.Y. contributed equally to this work and are listed in alphabetical order.

Author Contributions

S.F., P.Y., R.K., A.C., and M.D. conceived the project idea. S.F., R.K., and P.Y. prepared propylene carbonate VSe₂ suspensions. S.F. and P.Y. performed the TEM work. R.K. prepared diffraction simulation image. S.F. and P.Y. performed AFM measurements. P.Y. collected and analyzed Raman measurements. S.F. designed and created exfoliation apparatus (Cuvette_Holder.stl in Supplement). S.F., P.Y., and M.D. drafted the manuscript. S.F. and P.Y. prepared the figures and the Supporting Information. All authors have given approval to the final version of the manuscript.

Notes

The authors declare no competing financial interest.

■ ACKNOWLEDGMENTS

The authors thank David Evynshiteyn and Andrew Broeker for the design and printing of the holder for the tip magnetizer (Magnetotoaster.stl and ToasterFork.stl in Supplement). This work was supported by the NSF through the University of Pennsylvania Materials Research Science and Engineering Center (MRSEC) DMR-1720530 as well as NSF DMR 1905045, NSF EAGER 1838456, and DOE DE-SC0023224. This work was performed in part at the University of Pennsylvania's Singh Center for Nanotechnology, an NNCI member supported by NSF Grant ECCS-1542153.

■ ADDITIONAL NOTE

^aNote, the oxygen K line and the vanadium L line overlap substantially in EDS and could not be resolved, the zoomed-in spectra are presented in SI Figure S6.

■ REFERENCES

- (1) Gan, L. Y.; Zhang, Q.; Cheng, Y.; Schwingenschlögl, U. Two-dimensional ferromagnet/semiconductor transition metal dichalcogenide contacts: p-type Schottky barrier and spin-injection control. *Phys. Rev. B* **2013**, *88*, No. 235310.
- (2) Bonilla, M.; Kolekar, S.; Ma, Y.; Diaz, H. C.; Kalappattil, V.; Das, R.; Eggers, T.; Gutierrez, H. R.; Phan, M. H.; Batzill, M. Strong room-temperature ferromagnetism in VSe₂ monolayers on van der Waals substrates. *Nat. Nanotechnol.* **2018**, *13*, 289–293.
- (3) Fuh, H. R.; Chang, C. R.; Wang, Y. K.; Evans, R. F. L.; Chantrell, R. W.; Jeng, H. T. Newtype single-layer magnetic semiconductor in transition-metal dichalcogenides VX₂ (X = S, Se and Te). *Sci. Rep.* **2016**, *6*, No. 32625.
- (4) Fuh, H. R.; Chang, K. W.; Hung, S. H.; Jeng, H. T. Two-Dimensional Magnetic Semiconductors Based on Transition-Metal Dichalcogenides VX₂ (X = S, Se, Te) and Similar Layered Compounds VI₂ and Co(OH)₂. *IEEE Magn. Lett.* **2017**, *8*, 1–5.
- (5) Wang, L.; Tan, X.; Zhu, Q.; Dong, Z.; Wu, X.; Huang, K.; Xu, J. The universality applications of MoS₂@MnS heterojunction hollow microspheres for univalence organic or multivalence aqueous

electrolyte energy storage device. *J. Power Sources* **2022**, *518*, No. 230747.

(6) Xu, J.; Liu, Q.; Dong, Z.; Wang, L.; Xie, X.; Jiang, Y.; Wei, Z.; Gao, Y.; Zhang, Y.; Huang, K. Interconnected MoS₂ on 2D Graphdiyne for Reversible Sodium Storage. *ACS Appl. Mater. Interfaces* **2021**, *13*, 54974–54980.

(7) Xu, K.; Chen, P.; Li, X.; Wu, C.; Guo, Y.; Zhao, J.; Wu, X.; Xie, Y. Ultrathin Nanosheets of Vanadium Diselenide: A Metallic Two-Dimensional Material with Ferromagnetic Charge-Density-Wave Behavior. *Angew. Chem., Int. Ed.* **2013**, *52*, 10477–10481.

(8) Xue, Y.; Zhang, Y.; Wang, H.; Lin, S.; Li, Y.; Dai, J. Y.; Lau, S. P. Thickness-dependent magnetotransport properties in 1T VSe₂ single crystals prepared by chemical vapor deposition. *Nanotechnology* **2020**, *31*, No. 145712.

(9) Yang, J.; Wang, W.; Liu, Y.; Du, H.; Ning, W.; Zheng, G.; Jin, C.; Han, Y.; Wang, N.; Yang, Z.; Tian, M.; Zhang, Y. Thickness dependence of the charge-density-wave transition temperature in VSe₂. *Appl. Phys. Lett.* **2014**, *105*, No. 063109.

(10) Hossain, M.; Juanxia, W.; Wen, W.; Haining, L.; Xinsheng, W.; Liming, X. Chemical Vapor Deposition of 2D Vanadium Disulfide and Diselenide and Raman Characterization of the Phase Transitions. *Adv. Mater. Interfaces* **2018**, *5*, No. 1800528.

(11) Pásztor, A.; Scarfato, A.; Barreteau, C.; Giannini, E.; Renner, C. Dimensional crossover of the charge density wave transition in thin exfoliated VSe₂. *2D Mater.* **2017**, *4*, No. 041005.

(12) Strocov, V. N.; Shi, M.; Kobayashi, M.; Monney, C.; Wang, X.; Krempasky, J.; Schmitt, T.; Patthey, L.; Berger, H.; Blaha, P. Three-Dimensional Electron Realm in VSe₂ by Soft-X-Ray Photoelectron Spectroscopy: Origin of Charge-Density Waves. *Phys. Rev. Lett.* **2012**, *109*, No. 086401.

(13) Terashima, K.; Sato, T.; Komatsu, H.; Takahashi, T.; Maeda, N.; Hayashi, K. Charge-density wave transition of 1T-VSe₂ studied by angle-resolved photoemission spectroscopy. *Phys. Rev. B* **2003**, *68*, No. 155108.

(14) Feng, J.; Biswas, D.; Rajan, A.; Watson, M. D.; Mazzola, F.; Clark, O. J.; Underwood, K.; Markovic, I.; McLaren, M.; Hunter, A.; Burn, D. M.; Duffy, L. B.; Barua, S.; Balakrishnan, G.; Bertran, F.; Fevre, P. L.; Kim, T. K.; Van der Laan, G.; Hesjedal, T.; Wahl, P.; King, P. D. C. Electronic Structure and Enhanced Charge-Density Wave Order of Monolayer VSe₂. *Nano Lett.* **2018**, *18*, 4493–4499.

(15) Fumega, A. O.; Gobbi, M.; Dreher, P.; Wan, W.; González-Orellana, C.; Peña-Díaz, M.; Rogero, C.; Herrero-Martin, J.; Gargiani, P.; Ilyn, M.; Ugega, M.; Pardo, V.; Blanco-Canosa, S. Absence of Ferromagnetism in VSe₂ Caused by Its Charge Density Wave Phase. *J. Phys. Chem. C* **2019**, *123*, 27802–27810.

(16) Wong, P. K. J.; Zhang, W.; Bussolotti, F.; Yin, X.; Herng, T. S.; Zhang, L.; Huang, Y. L.; Vinai, G.; Krishnamurthi, S.; Bukhvalov, D. W.; Zheng, Y. J.; Chua, R.; N'Diaye, A. T.; Morton, S. A.; Yang, C. Y.; Tang, K. H. O.; Torelli, P.; Chen, W.; Goh, K. E. J.; Ding, J.; Lin, M. T.; Brocks, G.; Jong, M. P.; Castro Neto, A. H.; Wee, A. T. S. Evidence of Spin Frustration in a Vanadium Diselenide Monolayer Magnet. *Adv. Mater.* **2019**, *31*, No. 1901185.

(17) Gao, E.; Lin, S. Z.; Qin, Z.; Buehler, M. J.; Feng, X. Q.; Xu, Z. Mechanical exfoliation of two-dimensional materials. *J. Mech. Phys. Solids* **2018**, *115*, 248–262.

(18) Yu, W.; Li, J.; Herng, T. S.; Wang, Z.; Zhao, X.; Chi, X.; Fu, W.; Abdelwahab, I.; Zhou, J.; Dan, J.; Chen, Z.; Chen, Z.; Li, Z.; Lu, J.; Pennycook, S. J.; Feng, Y. P.; Ding, J.; Loh, K. P. Chemically Exfoliated VSe₂ Monolayers with Room-Temperature Ferromagnetism. *Adv. Mater.* **2019**, *31*, No. 1903779.

(19) Liu, Z. L.; Wu, X.; Shao, Y.; Qi, J.; Cao, Y.; Huang, L.; Liu, C.; Wang, J. O.; Zheng, Q.; Zhu, Z. L.; Ibrahim, K.; Wang, Y. L.; Gao, H. J. Epitaxially grown monolayer VSe₂: an air-stable magnetic two-dimensional material with low work function at edges. *Sci. Bull.* **2018**, *63*, 419–425.

(20) Li, D.; Wang, X.; Kan, C. M.; He, D.; Li, Z.; Hao, Q.; Zhao, H.; Wu, C.; Jin, C.; Cui, X. Structural Phase Transition of Multilayer VSe₂. *ACS Appl. Mater. Interfaces* **2020**, *12*, 25143–25149.

(21) Feroze, A.; Na, H. R.; Park, Y. C.; Jun, J. H.; Jung, M. H.; Lee, J. H.; Kim, J. H.; Seong, M. J.; Hong, S.; Chun, S. H.; Lee, S. In-Depth Structural Characterization of 1T-VSe₂ Single Crystals Grown by Chemical Vapor Transport. *Cryst. Growth Des.* **2020**, *20*, 2860–2865.

(22) Littlejohn, A. J.; Li, Z.; Lu, Z.; Sun, X.; Nawarat, P.; Wang, Y.; Li, Y.; Wang, T.; Chen, Y.; Zhang, L.; Li, H.; Kisslinger, K.; Shi, S.; Shi, J.; Raeliarijaona, A.; Shi, W.; Terrones, H.; Lewis, K. M.; Washington, M.; Lu, T. M.; Wang, G. C. Large Metallic Vanadium Disulfide Ultrathin Flakes for Spintronic Circuits and Quantum Computing Devices. *ACS Appl. Nano Mater.* **2019**, *2*, 3684–3694.

(23) Boscher, N. D.; Blackman, C. S.; Carmalt, C. J.; Parkin, I. P.; Prieto, A. G. Atmospheric pressure chemical vapour deposition of vanadium diselenide thin films. *Appl. Surf. Sci.* **2007**, *253*, 6041–6046.

(24) Zhang, Z.; Niu, J.; Yang, P.; Gong, Y.; Ji, Q.; Shi, J.; Fang, Q.; Jiang, S.; Li, H.; Zhou, X.; Gu, L.; Wu, X.; Zhang, Y. Van der Waals Epitaxial Growth of 2D Metallic Vanadium Diselenide Single Crystals and their Extra-High Electrical Conductivity. *Adv. Mater.* **2017**, *29*, No. 1702359.

(25) Yan, M.; Pan, X.; Wang, P.; Chen, F.; He, L.; Jiang, G.; Wang, J.; Liu, J. Z.; Xu, X.; Liao, X.; Yang, J.; Mai, L. Field-Effect Tuned Adsorption Dynamics of VSe₂ Nanosheets for Enhanced Hydrogen Evolution Reaction. *Nano Lett.* **2017**, *17*, 4109–4115.

(26) Zhao, W.; Dong, B.; Guo, Z.; Su, G.; Gao, R.; Wang, W.; Cao, L. Colloidal synthesis of VSe₂ single-layer nanosheets as novel electrocatalysts for the hydrogen evolution reaction. *Chem. Commun.* **2016**, *52*, 9228–9231.

(27) Xu, J.; Liu, Y.; Chen, P.; Wang, A.; Huang, K. J.; Fang, L.; Wu, X. Interlayer-expanded VS₂ nanosheet: Fast ion transport, dynamic mechanism and application in Zn²⁺ and Mg²⁺/Li⁺ hybrid batteries systems. *J. Colloid Interface Sci.* **2022**, *620*, 119–126.

(28) Xu, J.; Zhang, S.; Wei, Z.; Yan, W.; Wei, X.; Huang, K. Oriented VSe₂ nanoparticles anchored on N-doped hollow carbon sphere for high-stable aqueous energy application. *J. Colloid Interface Sci.* **2021**, *585*, 12–19.

(29) Gao, J.; Li, B.; Tan, J.; Chow, P.; Lu, T. M.; Koratkar, N. Aging of Transition Metal Dichalcogenide Monolayers. *ACS Nano* **2016**, *10*, 2628–2635.

(30) Li, Q.; Zhou, Q.; Shi, L.; Chen, Q.; Wang, J. Recent advances in oxidation and degradation mechanisms of ultrathin 2D materials under ambient conditions and their passivation strategies. *J. Mater. Chem. A* **2019**, *7*, 4291–4312.

(31) Diego, J.; Said, A. H.; Mahatha, S. K.; Bianco, R.; Monacelli, L.; Calandra, M.; Mauri, F.; Rossnagel, K.; Errea, I.; Blanco-Canosa, S. van der Waals driven anharmonic melting of the 3D charge density wave in VSe₂. *Nat. Commun.* **2021**, *12*, No. 598.

(32) Ramana, C. V.; Hussain, O. M.; Srinivasulu Naidu, B.; Julien, C.; Balkanski, M. Physical investigations on electron-beam evaporated vanadium pentoxide films. *Mater. Sci. Eng., B* **1998**, *52*, 32–39.

(33) Li, Q.; Yam, V. W. W. High-yield synthesis of selenium nanowires in water at room temperature. *Chem Commun.* **2006**, 1006–1008.